Mat. Res. Soc. Symp. Proc. Vol. 635 © 2001 Materials Research Society

Transport Properties of Bi-related Nanowire Systems

Y. M. Lin,[1] S. B. Cronin,[2] J. Y. Ying,[3] J. Heremans,[4] and M. S. Dresselhaus[1,2,*]
[1]Department of Electrical Engineering and Computer Science, [2]Department of Physics,
[3]Department of Chemical Engineering, Massachusetts Institute of Technology, Cambridge, MA 02139
[4]Delphi Research Labs, Delphi Automotive Systems, Warren, MI 48090
*On leave from the Massachusetts Institute of Technology, Cambridge, MA 02139

ABSTRACT

We present here an electrical transport property study of Te-doped Bi nanowires, and $Bi_{1-x}Sb_x$ alloy nanowires embedded in a dielectric matrix. The crystal structure of the nanowires were characterized by X-ray diffraction measurements, indicating that the nanowires possess the same lattice structure as bulk Bi in the presence of a small amount of Te or Sb atoms. The resistance measurements of 40-nm Te-doped Bi nanowires were performed over a wide range of temperature ($2\ K \leq T \leq 300\ K$), and the results are consistent with theoretical predictions. The 1D-to-3D localization transition and the boundary scattering effect are both observed in magneto-resistance measurements of $Bi_{1-x}Sb_x$ alloy nanowires at low temperatures ($T < 4$ K).

INTRODUCTION

Nanostructured materials have received much attention in the last decade because of their importance in fundamental studies and potential applications in diverse fields, such as chemistry, biology, optics, microelectronics, materials science, and thermoelectrics [1]. Various unusual phenomena and properties have been predicted and observed in nanoscaled materials. Among existing nanostructures, nanowires represent one of the most interesting systems because they exhibit stronger quantum confinement effects than 2D nanostructures such as superlattices, and they maintain structural continuity in one dimension, which allows for transport phenomena and they may serve as interconnections in future microelectronics applications.

Bismuth (Bi) is a very attractive material for the study of low-dimensional systems. Bi is a group V semimetal, in which the electrons are distributed in three highly anisotropic carrier pockets at the L points of the Brillouin zone, and the holes are contained in one pocket at the T point. The small energy overlap (38 meV at 77 K) in bulk Bi between the L-point conduction band and the T-point valence band is predicted to vanish in Bi nanowires when the diameter is smaller than ~50 nm, thus causing a semimetal-to-semiconductor transition [2]. Experimental results for this quantum-confinement-induced semimetal-semiconductor transition in Bi nanowires have been previously reported [3-4]. Since Bi has very small electron effective masses (~0.001 m_0 along the binary direction), quantum confinement effects can be observed at a larger scale (~50 nm), compared to less than 10 nm for most metals or semiconductors.

In addition to band shifts due to quantum confinement effects, it is also possible to controllably alter the energy-band structure and transport properties of Bi by alloying with another Group V element, Sb [5-6]. $Bi_{1-x}Sb_x$ alloys form substitutional solid solutions over the whole range of concentrations x. As x increases, the band structure of these alloys gradually transforms from that of Bi to that of Sb. Figure 1 shows a schematic representation of the band

structure of $Bi_{1-x}Sb_x$ as a function of x for $x < 0.3$. It is interesting to note that for $0.07 < x < 0.22$, the alloys are semiconductors with a direct or indirect band gap [7]. Therefore, $Bi_{1-x}Sb_x$ alloy nanowires constitute a promising 1D system in which the desired band structure and many other related properties can be achieved by combining the quantum confinement effect and the Sb alloying effect. Thus, many ideas that are central to the carrier pocket engineering concept [8] can be readily applied to this unique 1D system. Another important factor in optimizing electronic systems is the placement of the Fermi energy level in Bi nanowires. One possible approach to vary the Fermi energy is by doping with Group VI elements (e.g. Te), which serve as electron donors in $Bi_{1-x}Sb_x$ alloys, or Group IV elements (e.g. Pb, or Sn), which serve as electron acceptors.

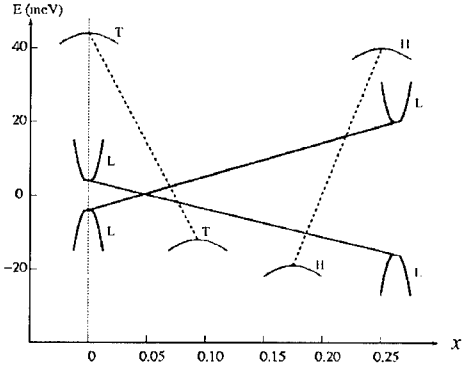

Figure 1. *The schematic diagram of the band structure of bulk $Bi_{1-x}Sb_x$ alloys as a function*

In the present work, the effects of adding Te or Sb to Bi nanowires are studied, both experimentally and theoretically. Bi nanowires for this study are synthesized by pressure injecting molten liquid metals into porous anodic alumina templates. In this fabrication method, it is straightforward to incorporate Te and Sb atoms in Bi nanowires by replacing the pure metal to be filled by the alloys of the desired composition. X-ray diffraction analysis of these nanowire arrays indicates that the lattice structures of the Bi-rich nanowires with a small amount of Te and Sb do not show significant differences from the undoped Bi nanowires. Temperature-dependent resistance $R(T)$ measurements are performed for $2\ K \leq T \leq 300\ K$ for the nanowire arrays using a two-point contact method. The experimental results exhibit good agreement with the theoretical calculations. The longitudinal magnetoresistance (MR) was studied as a function of applied magnetic field ($0\ T \leq B \leq 6\ T$) at various temperatures, and the localization effects are observed. For temperatures below 2 K, a 1D to 3D transition effect is noted. The non-monotonic behaviors in $MR(B)$ for larger-diameter nanowires are attributed to wire-boundary scattering effects, suggesting a high carrier mobility in these nanowires.

EXPERIMENTAL DETAILS

Bi, Te-doped Bi and $Bi_{1-x}Sb_x$ nanowire arrays were fabricated by a template-assisted approach, in which alumina templates consisting of hexagonally-packed arrays of nanopores

were used as the host material. The synthesis details and conditions to control the geometry of these nanopores have been described elsewhere [9-10]. The metal alloys used for the pressure injection were prepared by mixing high purity Bi (99.9999%, Alfa Aesar) and Te (99.9999 %, Alfa Aesar) or Sb (99.9999 %, Alfa Aesar) in a quartz tube, which was then evacuated and sealed. The sealed tube was heated to 650℃ for 8 hours with constant agitation to facilitate homogenizing the melt. The melt is then quenched in cold water. Bi-rich nanowires were produced by pressure injecting molten metals into the nanopores of the alumina templates, following similar procedures described in Ref. [11]. After the pressure injection, the underlying aluminum substrate and the barrier layer in the as-prepared nanowire templates are dissolved in a saturated $HgCl_2$ solution and a weak acid solution, respectively, so that the nanowires were exposed on both sides of the template and electrical contacts could be made to the nanowires.

Prior to the transport measurements, the as-prepared nanowire arrays were annealed at 250℃ for 8 hours to relieve the high pressure within the nanowires. Resistance and magnetoresistance measurements of the nanowire arrays were performed using a two-point contact method, in which gold wires were attached to both ends of the nanowires with silver paste. Typical resistances of the nanowire arrays range from tens of ohms to several thousand ohms. Since the number of wires connected to the contact electrodes in each set of samples would vary, the temperature dependence of the resistance of the various nanowire arrays were compared by normalizing the resistances to their respective values at 270 K.

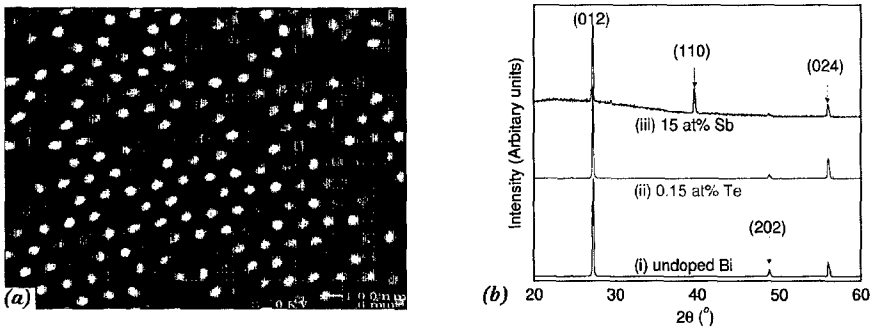

Figure 2. *(a) A SEM image of the bottom surface of an alumina template after the pressure injection filling process, showing arrays of Bi nanowires (white spots). (b) The XRD patterns of 40-nm Bi-rich nanowire arrays with different metal compositions.*

RESULTS AND DISCUSSION

Figure 2(a) shows a typical scanning electron microscopy (SEM) image of a bottom surface of the alumina template after the pressure injection filling process. The white spots represent pores filled by Bi or Bi alloys, and the dark spots are empty pore that have not been filled completely to the end of the pore. Figure 2(b) shows the x-ray diffraction (XRD) patterns for 40-nm nanowires arrays with different metal compositions. The XRD peaks of these nanowire arrays are assigned to the peaks of a Bi standard, showing that the lattice structures of Bi nanowires are not affected by the addition of Te (≤ 0.15 at%) and Sb (≤ 15 at%). The intensity

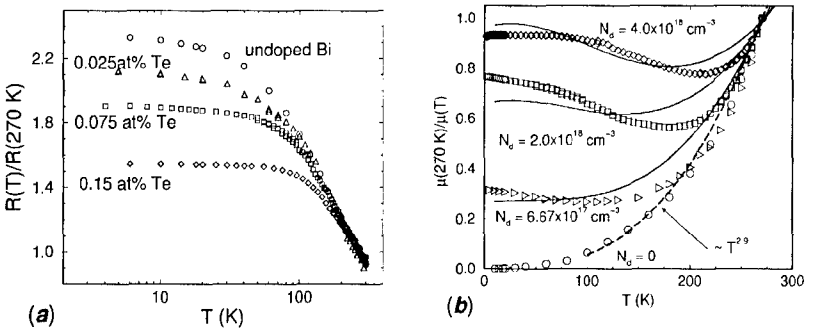

Figure 3. *(a) The measured R(T)/R(270 K) of 40-nm Bi nanowires with different nominal Te concentrations. (b) Experimental average carrier mobility of 40-nm Bi nanowires with different N_d and calculated results (solid curves).*

distributions of the peaks indicate that these nanowires possess a preferred crystal orientation perpendicular to the (012) lattice plane along the wire axes. The results are consistent with previous XRD studies on Bi nanowire arrays of various diameters [4], which show that there is a wire-diameter-dependent preferred crystal orientation along the wire axes for nanowires produced by pressure injection.

Figure 3(a) shows the measured $R(T)/R(270\ \mathrm{K})$ of 40-nm Bi nanowires with nominal Te concentrations based on the Bi/Te atomic ratio that was introduced in the melt to form the alloy. The actual Te concentration in the Bi nanowires is smaller than the nominal concentration due to the likely segregation of some Te atoms to the wire boundary during alloy solidification. Since the results are mainly dependent on the relative Te concentrations for the following discussions, we assume that 10% of the Te dopant in the alloy melt is present in the final nanowire product. With this assumption, 0.025 at%, 0.075 at%, and 0.15 at% Te-doped Bi alloys give rise to donor concentrations N_d of 6.67×10^{17}, 2.0×10^{18}, and $4.0\times10^{18}\ \mathrm{cm}^{-3}$ in the respective resulting nanowires. Based on the measured $R(T)$ in Fig. 3(a) and the calculated T-dependent carrier density, the T dependence of the average mobility μ_{avg} of these Te-doped Bi nanowires is obtained, shown as $\mu_{\mathrm{avg}}^{-1}(T)/\mu_{\mathrm{avg}}^{-1}(270\ \mathrm{K})$ in Fig. 3(b). μ_{avg}^{-1} of Te-doped Bi nanowires can be related to the various scattering processes using Matthiessen's rule by

$$\mu_{\mathrm{doped}}^{-1}(T) = \mu_{\mathrm{undoped}}^{-1}(T) + \mu_{\mathrm{imp}}^{-1}(T) + \mu_{\mathrm{defect}}^{-1}, \qquad (1)$$

where μ_{undoped} is the average mobility of the undoped Bi nanowires of the same diameter, and μ_{imp} and μ_{defect} are associated with the increased ionized impurity scattering and the expected higher defect level in Te-doped Bi nanowires, respectively. The average mobility of undoped Bi nanowires can be well fitted by a $\mu_{\mathrm{undoped}} \sim T^{-2.9}$ dependence for $T > 100$ K, as shown by the dashed line in Fig. 3(b), consistent with the predominant electron-phonon scattering at high T. The solid curves in Fig. 3(b) are the fitted results calculated from the transport models [2,4], showing good agreement with experimental results.

Figure 4(a) shows the longitudinal magnetoresistance of 40-nm $Bi_{0.85}Sb_{0.15}$ alloy nanowires as a function of magnetic field B at different temperatures. 40-nm nanowire samples with different Sb concentrations ($x = 0.05$ and 0.10) are also measured, and the results are similar to the ones shown in Fig. 4(a). At low fields, the magnetoresistance (MR) of most samples can be described by a parabolic relation

$$MR \equiv [R(B) - R(B=0)]/R(B=0) = A_0 B^2 \qquad (2)$$

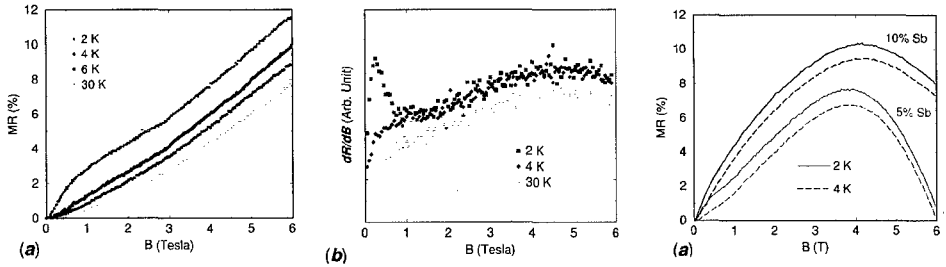

where A_0 is the magnetoresistance coefficient. For a single carrier (c) , A_0 is proportional to

Figure 4. *(a) Measured longitudinal magnetoresistance of 40-nm $Bi_{0.85}Sb_{0.15}$ alloy nanowires as a function of magnetic field B at different temperatures. (b) The first derivative with respect to the magnetic field B of the longitudinal magnetoresistance shown in (a). (c) Longitudinal magnetoresistance as a function of B for larger-diameter (d_w =65 nm) $Bi_{1-x}Sb_x$ nanowire arrays. The maximum in the MR is attributed to boundary scattering effects.*

the carrier mobility, while for a multiple carrier pocket system, A_0 is a complicated function of the mobility tensor elements. In Fig. 4(a), A_0 increases with decreasing temperature, consistent with a decreasing phonon scattering contribution as T decreases. It is noted that for $T < 4$ K, a plateau in the magnetoresistance is observed around $B = 0.7$ T. This abnormal feature can be more readily seen in the first derivative of the magnetoresistance, as shown in Fig. 4(b). The same behavior was also observed for other 40-nm nanowires with different Sb concentrations. This plateau feature is attributed to the 1D-to-3D localization effect at which the magnetic length equals the wire diameter, as described in Ref. [12].

Figure 4(c) shows the magnetoresistance as a function of magnetic field for larger-diameter (d_w = 65 nm) $Bi_{1-x}Sb_x$ nanowire arrays. The 1D-to-3D localization effect, although weaker than that in the 40-nm nanowires, can also be observed at a lower magnetic field. Another interesting feature is the non-monotonic *MR*(*B*) and a maximum in the longitudinal *MR*, which are attributed to boundary scattering effects [13]. In the presence of magnetic fields, the trajectory of the carriers will be deflected, which increases the probability of boundary scattering. However, as the magnetic fields increase beyond a critical field such that the cyclotron orbits of the carriers lie within the wires, the frequency of the boundary scattering events will be reduced, resulting in a decrease in the longitudinal *MR*. We note that this maximum in the magnetic field due to the boundary scattering mainly depends on the wire diameter, as indicated by the curves shown in Fig. 4(c) for two different Sb concentrations. We also note that $Bi_{0.9}Sb_{0.1}$ nanowires have a larger magnetoresistance maximum than $Bi_{0.95}Sb_{0.05}$ nanowires. One major reason for the difference in the *MR* maximum in 65-nm nanowires of different Sb concentrations may be due to the increased boundary scattering with increasing Sb concentrations. It is expected that the introduced Sb atoms in Bi nanowires will migrate to the wire surface during the alloy solidification and subsequent annealing processes. Thus, nanowires with a higher Sb concentration tend to exhibit higher neutral impurity and defect densities near the wire boundary. Therefore, for a moderate magnetic field lower than the critical field, carriers traveling along the wire will experience more scattering events, resulting in a larger increase in the *MR*. However, it should be noted that in addition to the increased neutral impurity scattering, the introduction of Sb varies the relative population of different carrier pockets in Bi nanowires, which may also contribute to the change in the average carrier mobility and to the different

curvatures shown in Fig 4(c). Efforts are being made to acquire a more accurate determination of the Sb concentration and spatial distributions of the dopants in the nanowires in order to obtain a quantitative and more detailed understanding of the effect of Sb alloying in Bi nanowires.

CONCLUSIONS

We have synthesized Bi, Te-doped Bi, and $Bi_{1-x}Sb_x$ alloy nanowire arrays in anodic alumina templates, and studied their transport properties over a wide range of temperatures and magnetic fields. The XRD patterns of the nanowire arrays indicate that the Bi lattice structure is not altered by the Te or Sb atoms introduced. The *T*-dependent resistance measurements of Te-doped nanowires are consistent with theoretical calculations. The 1D-to-3D localization effect and the boundary scattering effect are observed in $Bi_{1-x}Sb_x$ alloy nanowires at low temperatures ($T < 4$ K), suggesting a high carrier mobility in the nanowires.

ACKNOWLEDGMENTS

We thank Dr. G. Dresselhaus at MIT and Prof. G. Chen at UCLA for valuable discussions. The support from MURI Subcontract No. 0205-G-74114-01, NSF Grant No. DMR-98-04734, and U. S. Navy Contract No. N00167-92-K005 is gratefully acknowledged.

REFERENCES

1. L. D. Hicks and M. S. Dresselhaus, Phys. Rev. B **47**, 12727 (1993).
2. Y.-M. Lin, X. Sun and M. S. Dresselhaus, Phys. Rev. B **62**, 4610 (2000).
3. J. Heremans, C. M. Thrush, Yu-Ming Lin, S. Cronin, Z. Zhang, M. S. Dresselhaus and J. F. Mansfield, Phys. Rev. B **61**, 2921 (2000).
4. Y.-M. Lin, S. B. Cronin, J. Y. Ying, M. S. Dresselhaus, and J. P. Heremans, Appl. Phys. Lett. **76**, 3944 (2000).
5. H. J. Goldsmid, Phys. Stat. Sol. (a) **1**, 7 (1970).
6. B. Lenoir, A. Dauscher, X. Devaux, R. Martin-Lopez, Yu. I. Ravich, H. Scherrer and S. Scherrer, in *Proceedings of the 15th International Conference on Thermoelectrics* (IEEE, 1996), pp. 1.
7. M. S. Dresselhaus, J. Phys. Chem. Sol. **32**, Suppl. 1, 3 (1971).
8. T. Koga, X. Sun, S. B. Cronin and M. S. Dresselhaus, Appl. Phys. Lett. **73**, 2950 (1998).
9. F. Keller, M. S. Hunter, D. L. Robinson, J. Electrochem. Soc. **100**, 411 (1953).
10. F. Y. Li, L. Zhang, R. M. Metzger, Chem. Mater. **10**, 2470 (1998).
11. Z. Zhang, J. Y. Ying and M. S. Dresselhaus, J. Mater. Res. **13**, 1745 (1998).
12. J. Heremans, C. M. Thrush, Z. Zhang, X. Sun, M. S. Dresselhaus, J. Y. Ying and D. T. Morelli, Phys. Rev. B, **58**, R10091 (1998).
13. Z. Zhang, X. Sun, M. S. Dresselhaus, J. Y. Ying and J. Heremans, Phys. Rev. B **61**, 4850 (2000).